iJRASET
International Journal For Research in Applied Science and Engineering Technology

INTERNATIONAL JOURNAL FOR RESEARCH

IN APPLIED SCIENCE & ENGINEERING TECHNOLOGY

Volume: 11 **Issue:** III **Month of publication:** March 2023

DOI: https://doi.org/10.22214/ijraset.2023.49578

www.ijraset.com

Call: 08813907089 | E-mail ID: ijraset@gmail.com

International Journal for Research in Applied Science & Engineering Technology (IJRASET)
ISSN: 2321-9653; IC Value: 45.98; SJ Impact Factor: 7.538
Volume 11 Issue III Mar 2023- Available at www.ijraset.com

A QUASI-Z-SOURCE Converter Using a Single-Stage Switched-Inductor Boost DC-DC Converter

Mrs. J. Sravanthi[1], Mrs. A. Anuradha[2]
[1]*PG scholar in the Dept. of Electrical & Electronics Engineering, in Holy Mary Institute of Technology & Science, Bogaram (V), Medchal District, Hyderabad, India.*
[2]*Assistant Professor in the Dept. of Electrical & Electronics Engineering, in Holy Mary Institute of Technology & Science, Bogaram (V), Medchal District, Hyderabad, India.*

Abstract: ***This paper introduces a new topology, yet simple and efficient, for a grid-connected wind-solar cogeneration system. A permanent magnet synchronous generator-based full-scale wind turbine is interconnected to the utility grid. The dc-link capacitor has been utilized to directly interface a photovoltaic solar generator. No dc/dc conversion stages are required, and hence, the hybrid system is simple and efficient. Moreover, the proposed topology features an independent maximum power point tracking for both the wind and the solar generators to maximize the extraction of renewable energy. This paper presents a quasi-Z-source inverter (qZSI) that is a new topology derived from the traditional Z-source inverter (ZSI). The qZSI inherits all the advantages of the ZSI, which can realize buck/boost, inversion and power conditioning in a single stage with improved reliability. In addition, the proposed qZSI has the unique advantages of lower component ratings and constant dc current from the source. All of the boost control methods that have been developed for the ZSI can be used by the qZSI. One of the more commonly used techniques is the incremental conductance method. In this paper, an improved particle swarm optimization-(IPSO-) based MPPT technique for photovoltaic system operating under varying environmental conditions is proposed. Basically, an Artificial Neural Network (ANN) based approach is utilized to automatically detect the global maximum power point of the PV array by using a preselected number of power measurements of the PV system. The approach of linearly decreasing scheme for weighting factors and cognitive and social parameters is modified. The proposed control scheme can overcome deficiency and accelerate convergence of the IPSO-based MPPT algorithm. Detailed small-signal models for the system components are developed to characterize the overall stability. The influence of the utility-grid faults on the performance of the proposed system is also investigated. Nonlinear time-domain simulation results under different operating conditions are presented to validate the effectiveness of the proposed topology.***

Keywords: AC-DC power converters, DC-AC power converters, maximum power point trackers, permanent magnet machines, solar power generation, wind power generation

I. INTRODUCTION

The cost of the wind and solar generation has been rapidly falling since the last decade. Driven by their economic and technical incentives, the global installed solar and wind power capacity has approached 303 Gigawatt (GW) and 487 GW in 2016, as compared to 6 GW and 74 GW in 2006, respectively [1]. Due to the intermittent and unregulated nature of the wind and solar energy, power-electronic converters are utilized as an interfacing stage to the load-side or the utility-grid to create distributed generation units [2], [3]. In the literature, most of the distributed generation systems are solely dedicated for one form of renewable resources, e.g., a solar energy as in [4], [5] or a wind energy as presented in [6]–[8]. In order to maximize the benefits of the available renewable resources, the combination of the wind and solar generators in one location has been recently considered [9]–[22].

The hybrid wind and solar energy cogeneration features the following characteristics; 1) the availability of the wind and solar energy is generally complementary, and hence combining both forms of energy increases the overall operational efficiency [23]. 2) the hybrid wind and solar co-generators optimize the utilization of lands resources due to the reduced footprint of the combined system, and hence improves the capital investments [24]. 3) as compared to the static solar generators, the combined wind and solar cogeneration systems are more dynamically capable to support the utility-grid thanks to the available moment of inertia in the mechanical parts of the wind generators [8]. 4) having two sources of energy increases the generation reliability [9], [10]. In the literature, the grid-connected wind and solar cogenerators are not widely addressed [9]–[15]. On the contrary, several wind and solar hybrid systems are available for the standalone off-grid applications [10], [16]–[22].

An optimal sizing method for a wind-solar-battery system in the grid-connected and standalone applications has been proposed in [10]. A systematic stochastic planning for a hybrid system consisting of the wind and solar systems is proposed in [11]. In [12]–[14], the integration of the renewable energy resources has been improved by utilizing multiple-input converters. A buck/buck-boost fused dc-dc converter is proposed in [12]. A dc-dc converter with a current-source interface, and a coupled transformer are proposed in [13] and [14], respectively. Beside the relatively complex structured topologies in [12]–[14], the proposed systems are based on the dc power distribution which might not be the ideal distribution medium in the ac-dominated power systems. Moreover, the introduced systems are proposed for relatively low-power levels and have not been tested in high-power applications. A standalone hybrid wind and solar system is proposed in [16], [17] including a diesel engine generator and a storage battery. On the small-scale level, a single phase hybrid system has been proposed in [18] whereas a laboratory-scale system is introduced in [19], [20]. Generally, the system structure in [16]–[20] comprises a common dc-bus that interfaces several parallel connected converters-interfaced renewable energy resources, which might reduce the overall system efficiency and increase the cost [12]. Moreover, the cascaded connection of power converters requires rigorous controllers design and coordination to avoid the induced interactions dynamics among the tightly regulated power converters, which might yield instabilities [25], [26]. A back-to-back (BtB) voltage-source converter (VSC) connected to a doubly-fed induction generator is used to interface a dc-dc converter-interfaced photovoltaic (PV) generator and an energy storage unit in [21]. In [22], a PV generator charging a battery bank and interfaced to a wind driven induction generator via a VSC is proposed. The hybrid wind-solar systems in [21], [22] highlights the efficient integration of the renewable energy resources with the minimal utilization of power electronic conversion stages. However, these systems are proposed for specific off-grid applications. Up to the authors' best knowledge, the combination of the grid-connected wind-solar systems has been mainly addressed in [15].

The Z-source inverter (ZSI) has been reported suitable for residential PV system [1-2] because of the capability of voltage boost and inversion in a single stage. Recently, four new topologies, the quasi-Z-source inverters (qZSI), have been derived from the original ZSI [3]. This paper analyzes one voltage fed topology of these four in detail and applies it to PV power generation systems. By using the new quasi-Zsource topology, the inverter draws a constant current from the PV array and is capable of handling a wide input voltage range. It also features lower component ratings and reduced source stress compared to the traditional ZSI. A prototype which provides three phase 60-Hz, 208-Vllrms ac has been built in laboratory. It is demonstrated from the theoretical analysis, simulation and experimental results that the proposed qZSI can realize voltage buck or boost and dc-ac inversion in a single stage with high reliability and efficiency, which makes it well suited for PV power systems.

An alternative approach is to employ evolutionary algorithm (EA) techniques. Due to its ability to handle nonlinear objective functions [13], EA is envisaged to be very effective to deal with MPPT problem. Among the EA techniques, particle swarm optimization (PSO) is highly potential due to its simple structure, easy implementation, and fast computation capability [13]. Since PSO is based on search optimization, in principle, it should be able to locate the MPP for any type of *P-V* curve regardless of environmental variations. It can be used to track the MPP of PV system as the search space of the PSO is reduced, and, hence, the time required for convergence can be greatly decreased. Interestingly, one important feature of the PSO which is ignored by researchers [5, 6, 13, 14] is the searching speed through adaptive learning factors and inertia weight. Linear decreases in line with increasing iteration numbers were adopted in this study for the weighting of the PSO formulas. The physical meaning of this modified weighting formula is that greater step sizes are used to increase the particle search velocity during the initial search because the distance to the global optimum is relatively large. This prevents an excessively small step size from making local optimum traps unavoidable. The system in [15] comprises a BtB VSCs to interface the solar and wind generators to the utility-grid. On the machine-side-VSC, the dc-link voltage is regulated to the maximum power-point tracking (MPPT) value of the PV panel by an outer loop Proportional-and-Integral (PI) dc voltage controller. The reference values of the machine-side currents are calculated using the synchronous detection method, and a hysteresis current controller is utilized for the regulation. On the grid-sideVSC, a hysteresis grid-current controller is used to inject the total currents to the utility-grid. In spite of the potential benefits of the proposed system in [15], the following challenges are noted; 1) the MPPT of either the PV and wind power involves the operation of both VSCs, which in some cases might decrease the system reliability and increase the losses. Actually, ANNs have been already applied to MPPT problems, but it is the first time that ANNs are used to identify the GMPP as proposed in this paper, far as authors know. The other ANN based MPPT algorithms presented in past literature are usually exploited to compensate the parameter variations occurring in the PV system in the identification of local MPPs [14–18]. On the other hand, the ANN based MPPT method presented in [32] estimates the GMPP by means of a single voltage and current measurement but the study is limited to a very restricted number of shading combinations, thus it is few practicable for a generic PV system especially when it is continuously subjected to very fast changing and not uniform shading conditions.

For instance, if the wind velocity is lower than the cut-off speed of the wind turbine, i.e., no wind power, the machine-side VSC may be unable to track the solar PV MPPT dc-link voltage [15]. 2) the dc-link voltage is regulated from the machine-side, and there is no a direct regulation on the speed of the wind turbine, i.e., a servo operation. 3) the machine and grid-side currents are controlled using hysteresis controllers resulting in a variable switching frequency and higher harmonic contents. Motivated by the promising benefits of the hybrid wind-solar generation systems, and the challenges facing the proposed system in [15], this paper introduces a new topology, yet simple and efficient to interface both the wind and solar generators into the utility-grid. The contributions of this paper are as follows: 1) The realization of the combined grid-connected wind and solar generators using BtB VSCs with no extra power electronic switches. 2) Unlike the proposed system in [15], the voltage-source rectifier (VSR) is solely responsible for MPPT of the wind generator whereas the voltage-source inverter (VSI) harvests the maximum PV power by regulating the dc-link voltage to inject the total dc power into the utility-grid. 3) The development of the entire small-signal state-space model of the proposed system to characterize the overall system stability. 4) The performance of proposed hybrid system has been investigated under different operating conditions including the utility-grid faults using time-domain simulations.

II. CIRCUIT ANALYSIS OF THE QUASI-Z-SOURCE INVERTER

Quasi-Z-Source Inverter Circuit Figs. 1a and 1b show the traditional voltage fed ZSI [4] and the proposed voltage fed qZSI, respectively. In the same manner as the traditional ZSI, the qZSI has two types of operational states at the dc side: the nonshoot-through states (i.e. the six active states and two conventional zero states of the traditional VSI) and the shoot-through state (i.e. both switches in at least one phase conduct simultaneously). In the non-shoot-through states, the inverter bridge viewed from the dc side is equivalent to a current source. The equivalent circuits of the two states are as shown in Figs. 2a and 2b. The shoot-through state is forbidden in the traditional VSI, because it will cause a short circuit of the voltage source and damage the devices. With the qZSI and ZSI, the unique LC and diode network connected to the inverter bridge modify the operation of the circuit, allowing the shoot-through state. This network will effectively protect the circuit from damage when the shoot-through occurs and by using the shoot-though state, the (quasi-) Z-source network boosts the dc-link voltage. The major differences between the ZSI and qZSI are (1) the qZSI draws a continuous constant dc current from the source while the ZSI draws a discontinuous current and (2) the voltage on capacitor C2 is greatly reduced. The continuous and constant dc current drawn from the source with this qZSI make this system especially well suited for PV power conditioning systems.

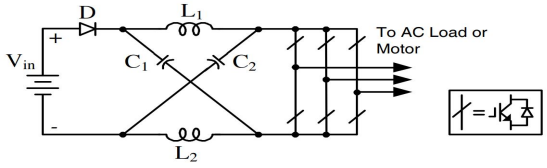

Figure 1. Voltage fed Z-source inverter

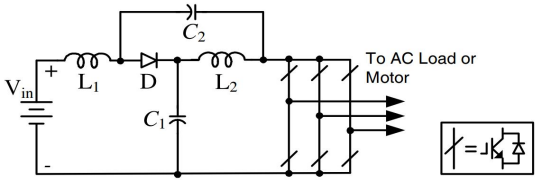

Figure2. Voltage fed quasi-Z-source inverter

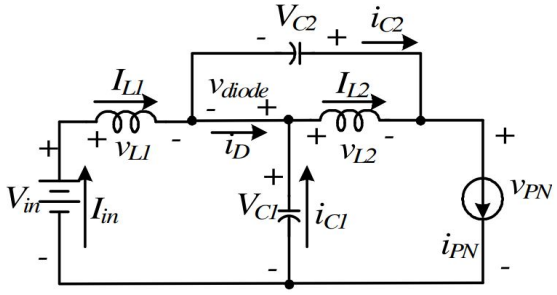

Figure 3 Equivalent circuit of the qZSI in non-shoot-through states

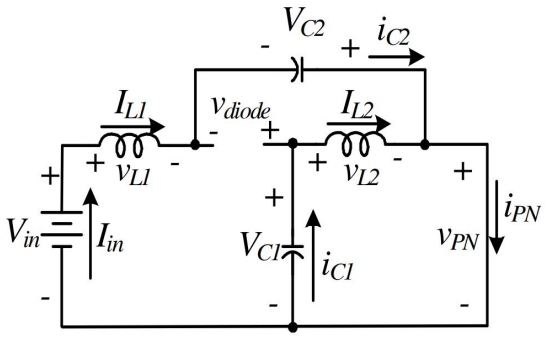

Figure 4. Equivalent circuit of the qZSI in shoot-through states

A. Circuit Analysis

All the voltages as well as the currents are defined in Figs 2a, 2b and the polarities are shown with arrows. Assuming that during one switching cycle, T , the interval of the shootthrough state is T0 ; the interval of non-shoot-through states is T1 ; thus one has T = T0 + T1 and the shoot-through duty ratio, D = T0 /T . From Fig 2a which is a representation of the inverter during the interval of the non-shoot-through states, T1 , one can get

$v_{L1} = V_{in} - V_{C1}$, $v_{L2} = -V_{C2}$, and

$v_{PN} = V_{C1} - v_{L2} = V_{C1} + V_{C2}$ $v_{diode} = 0$.

From Fig 2b which is a representation of the system during the interval of the shoot-through states, T0 , one can get

$v_{L1} = V_{C2} + V_{in}$, $v_{L2} = V_{C1}$, and

$v_{PN} = 0$ $v_{diode} = V_{C1} + V_{C2}$.

At steady state, the average voltage of the inductors over one switching cycle is zero. From (1), (3), one has

$$\begin{cases} V_{L1} = \bar{v}_{L1} = \dfrac{T_0(V_{C2} + V_{in}) + T_1(V_{in} - V_{C1})}{T} = 0 \\ V_{L2} = \bar{v}_{L2} = \dfrac{T_0(V_{C1}) + T_1(-V_{C2})}{T} = 0 \end{cases}$$

$$V_{C1} = \frac{T_1}{T_1 - T_0} V_{in}$$

$$V_{C2} = \frac{T_0}{T_1 - T_0} V_{in}$$

From (2), (4) and (5), the peak dc-link voltage across the inverter bridge is

$$\hat{v}_{PN} = V_{C1} + V_{C2} = \frac{T}{T_1 - T_0} V_{in} = \frac{1}{1 - 2\frac{T_0}{T}} V_{in} = BV_{in}$$

where B is the boost factor of the qZSI. This is also the peak voltage across the diode. The average current of the inductors L1 , L2 can be calculated by the system power rating P

$$I_{L1} = I_{L2} = I_{in} = P / V_{in}$$

According to Kirchhoff's current law and (7), we also can get that

$$I_{C1} = I_{C2} = I_{PN} - I_{L1} \qquad I_D = 2I_{L1} - I_{PN}$$

In summary, the voltage and current stress of the qZSI are shown in Table 1. The stress on the ZSI is shown as well for comparison, where (1) M is the modulation index; ln v^ is the ac peak phase voltage; P is the system power rating;

(2) $m = T_1/(T_1 - T_0)$; $n = T_0/(T_1 - T_0)$; thus $m > 1; m - n = 1$;

(3) $B = T/(T_1 - T_0)$, thus $m + n = B$, $1 < m < B$.

From Table 1 we can find that the qZSI inherits all the advantages of the ZSI. It can buck or boost a voltage with a given boost factor. It is able to handle a shoot through state, and therefore it is more reliable than the traditional VSI. It is unnecessary to add a dead band into control schemes, which reduces the output distortion. In addition, there are some unique merits of the qZSI when compared to the ZSI:

Table 1 Voltage and average current of the qZSI and ZSI network

	$v_{L1} = v_{L2}$		v_{PN}		v_{diode}	
	T_0	T_1	T_0	T_1	T_0	T_1
ZSI	mV_{in}	$-nV_{in}$	0	BV_{in}	BV_{in}	0
qZSI	mV_{in}	$-nV_{in}$	0	BV_{in}	BV_{in}	0
	V_{C1}		V_{C2}		$\hat{v}_{\ln}$	
ZSI	mV_{in}		mV_{in}		$MBV_{in}/2$	
qZSI	mV_{in}		nV_{in}		$MBV_{in}/2$	
	$I_{in} = I_{L1} = I_{L2}$		$I_{C1} = I_{C2}$		I_D	
ZSI	P/V_{in}		$I_{PN} - I_{L1}$		$2I_{L1} - I_{PN}$	
qZSI	P/V_{in}		$I_{PN} - I_{L1}$		$2I_{L1} - I_{PN}$	

1) The two capacitors in ZSI sustain the same high voltage; while the voltage on capacitor C2 in qZSI is lower, which requires lower capacitor rating;
2) The ZSI has discontinuous input current in the boost mode; while the input current of the qZSI is continuous due to the input inductor L1 , which will significantly reduce input stress;
3) For the qZSI, there is a common dc rail between the source and inverter, which is easier to assemble and causes less EMI problems.

III. ANFIS FUZZY CONTROLLER TYPE TAKAGI-SUGENO

The fuzzy models Takagi-Sugeno are renowned for being an efficient technique to represent a non-linear system with fuzzy sets and fuzzy reasoning. Like the Mamdani model, this type of model builds using a base of rules of the type "If … then …" where
if the antecedent is always linguistically expressed, the consequent uses numerical variables rather than linguistic variables. The consequent may be expressed, for instance, as a constant, a polynome or, more generally, as a function or a differential equation depending on variables associated with the antecedent. Generally, the model type Takagi-Sugeno is based on a collection of rules Ri of the type:

$$Ri: \text{If } (E \text{ est } Ai) \text{ And } (\Delta E \text{ est } Bi) \text{ Then } yi = fi(E, \Delta E) \text{ for } i = 1, 2, \cdots, n$$

where Ride notes the ith rule of the model and n the number of fuzzy rules that the base of rules contains. E and ΔE are the input variables x, called antecedents, and y is the output variable, called consequent.
Ai and Bi are fuzzy sets of the antecedent of the nth rule. These fuzzy rules are defined by membership functions $\mu_{Ai}(E)$ or $\mu_{Bi}(\Delta E)$ belonging to the interval [0, 1]. $\mu_{Ai}(E)$ or $\mu_{Bi}(\Delta E)$ symbolize the value of membership functions of the input E or the input ΔE respectively to the fuzzy set Ai or Bi.
In the case where the consequents yi = fi(E, ΔE) take the form of a constant, which corresponds to our study case (yi = Δα), the model is called singleton or zero order.
The suggested fuzzy logic controller to optimize the system, is represented in Figure 6. It receives as input the error and the error variation of the system (E(k), ΔE(k)). In the output, the variation of the duty cycle is generated Δα driving the DC-DC converter.

This controller can be split in three principal modules:
1) *Input:* Fuzzification. It associates a membership degree ranging from 0 and 1 with each of the real inputs.
2) *Inference Engine:* It is associated to the base of rules type: "If … then …".
3) *Output:* Defuzzification. It permits the transformation of the membership degrees of fuzzy sets into numerical values.

Our fuzzy controller presented in Figure 7 is characterized by:

a) Two inputs: error E and its variation ΔE and one output Δα.
b) Scaling factors K_1 and K_2 (from −1 to 1) for the normalization of inputs associated with the error and its variation.
c) The universe of discourse divided into five classes, further described below, for the input and output variables.
d) Triangular and trapezoidal membership functions.

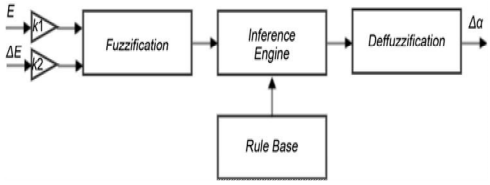

Figure 5. Fuzzy controller structure.

e) Involvement of Takagi-Sugeno for inference.
f) The weighted average method for the calculation of the output.

The two input variables E and ΔE are defined by the two following expressions:

$$E = \frac{\Delta P_{pv}}{\Delta V_{pv}} = \frac{P_{pv}(t) - P_{pv}(t-1)}{V_{pv}(t) - V_{pv}(t-1)}.$$

$$\Delta E = E(t) - E(t-1).$$

The controller output Δα is defined by the control law which depends on the error E and its ΔE as follows:

$$\Delta\alpha = f(E, \Delta E).$$

And the duty cycle α, which drives the DC-DC converter, is expressed by:

$$\alpha(t) = \alpha(t-1) + \Delta\alpha.$$

The big advantage of the Takagi-Sugeno technique is that it permits to simplify the aggregation calculation, so that we can not only obtain a simple solution more rapidly but also alleviate the global calculation mechanism significantly.
In the Takagi-Sugeno modelling, the final output is equal to the weighted average of the output of each rule. This average is given by the following expression:

$$CG_{Sugeno} = \frac{\sum_{i=1}^{n} z_i w_i}{\sum_{i=1}^{n} w_i}.$$

where z_i is the output level of each rule R_i and w_i is the membership calculated by the following equation:

$$w_i = \mu_{Ai}(E) \cdot \mu_{Bi}(\Delta E).$$

The rules base is summarized in Table 3. In our system case, the universe of dis- course is divided into five classes NL, NS, ZO, PS and PL, for the input and output variables as follows: NL for negative large, NS for negative small, ZO for zero, PS for positive small and PL for positive large.
The membership functions used in the case of our fuzzy controller are of triangular and trapezoidal types for the input, but of singleton type for the output.

IV. EVALUATION RESULTS

A time-domain simulation model for the hybrid system in Fig. 1 is developed under the Matlab/Simulink environment to evaluate the validity and the performance of the system. The wind and solar generators are rated at 2.0 and 0.9 MVA, respectively. The complete model entities are built using the SimPowerSystem toolbox. The VSCs are simulated using average-model-based blocks. The simulation type is discrete with a sample time of 50 μs. In the following subsections, the proposed hybrid system is subjected to theoretical challenging operating conditions which might not occur in the realty, e.g., large step variations in the wind speed and the solar irradiance levels, and three-phase-toground (3PG) faults conditions. The external disturbances have been applied in the worst case to challenge the system stability and show the effectiveness of the designed controllers.

A. Small-Signal Model Verification

The accuracy of the small-signal state-space model in (17) is validated in Fig. 4 following a 5.0% step increase in Vdc at t = 1.0 s. Originally, the system controllers are designed such that a highly damped performance is yielded. However, a lightly damped response has been induced by increasing the bandwidth of the dc-link voltage controller so that the model can be easily validated. For an eigenvalue $\lambda = -\sigma \pm j\omega\lambda$, the frequency of oscillation is $\omega\lambda$ [in rad/s] whereas the envelope of the oscillatory response decays following the exponential function $A\lambda\exp(-\sigma t)$, where $A\lambda$ is the amplitude of the oscillation and tis the time in seconds. From (17), the yielded dominant lightly-damped mode is $\lambda = -73.03 \pm j251.7$. Referring to Fig. 4, the frequency of the oscillation of the same lightly-damped response is 247.4 rad/s whereas the oscillatory response decays following a close match to $A\lambda\exp(-73.03t)$, which implies the accurate development of the small-signal model in (17).

B. Wind and Solar Co-Generation

The co-generation of the wind and solar energy is investigated following different weather conditions. As shown in Fig. 5(a), the wind speeds increases from 8.4 to 10.8, then drops to 7.2, and finally increases to 12 m/s at t = 2, 4, and 6 s, respectively. Along with the wind speed variations, the solar irradiance level decreases from 1 to 0.8, and then 0.4, and finally increases to 0.6 kW/m2 , at t = 3, 5, and 6 s, respectively. Following Figs. 2 and 3, the MPPTw and MPPTs generate the optimal $\omega * r$ and $V * dc$. As shown in Figs. 5(b) and (c), both ωr and Vdc have a welldamped performance which is reflected on the generated wind and solar power as depicted in Figs. 5(d) and (e), respectively, and the injected current to the utility-grid as in Fig. 5(f). For further investigations, the maximum wind power, i.e., 2 MW, and a solar power of 0.568 MW are generated at t = 6.0 s where the dc-link stability is preserved with a maximum overshot of 0.06 p.u. Under all conditions, a unity PCC voltage is maintained as shown in Fig. 5(g). The designed controllers for the hybrid wind-solar system do not saturate the pulse-width modulation of the BtB VSCs as shown in Figs. 5(h) and (i), where the variable frequency operation of the VSR is clearly noted.

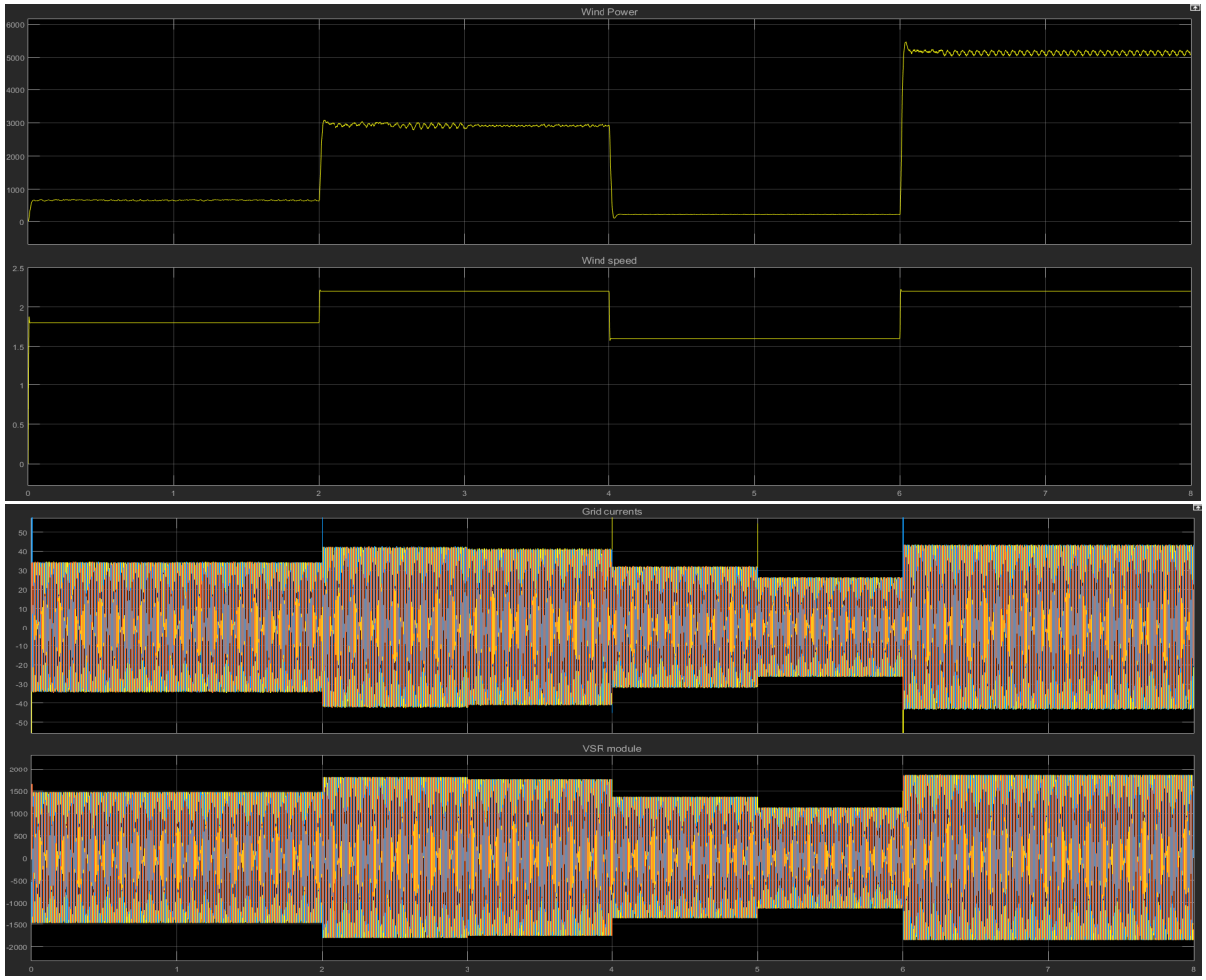

Fig. 6. Performance of the wind and solar generators.

C. Wind-Only Generation

During the night-time at low-irradiance conditions, the PV generator provides zero (or negligible) power to the utility-grid. Under these conditions, the dc-link voltage controller regulates Vdc to the minimum value following the PV characteristics in Fig. 3. As shown in Fig. 6(a), the dc-link voltage drops to 0.858 p.u. at t = 2.0 s as the PV power generation drops to 0, and is restored back to 1.0 p.u. at t = 3.0 s when the PV power is generated. The corresponding wind and solar power as well as the injected ac current to the utility-grid are shown in Figs. 6(b)and (c), respectively. Note that a blocking diode is usually connected in series with each PV string to prevent reverse current flowing into the PV array at low irradiance levels.

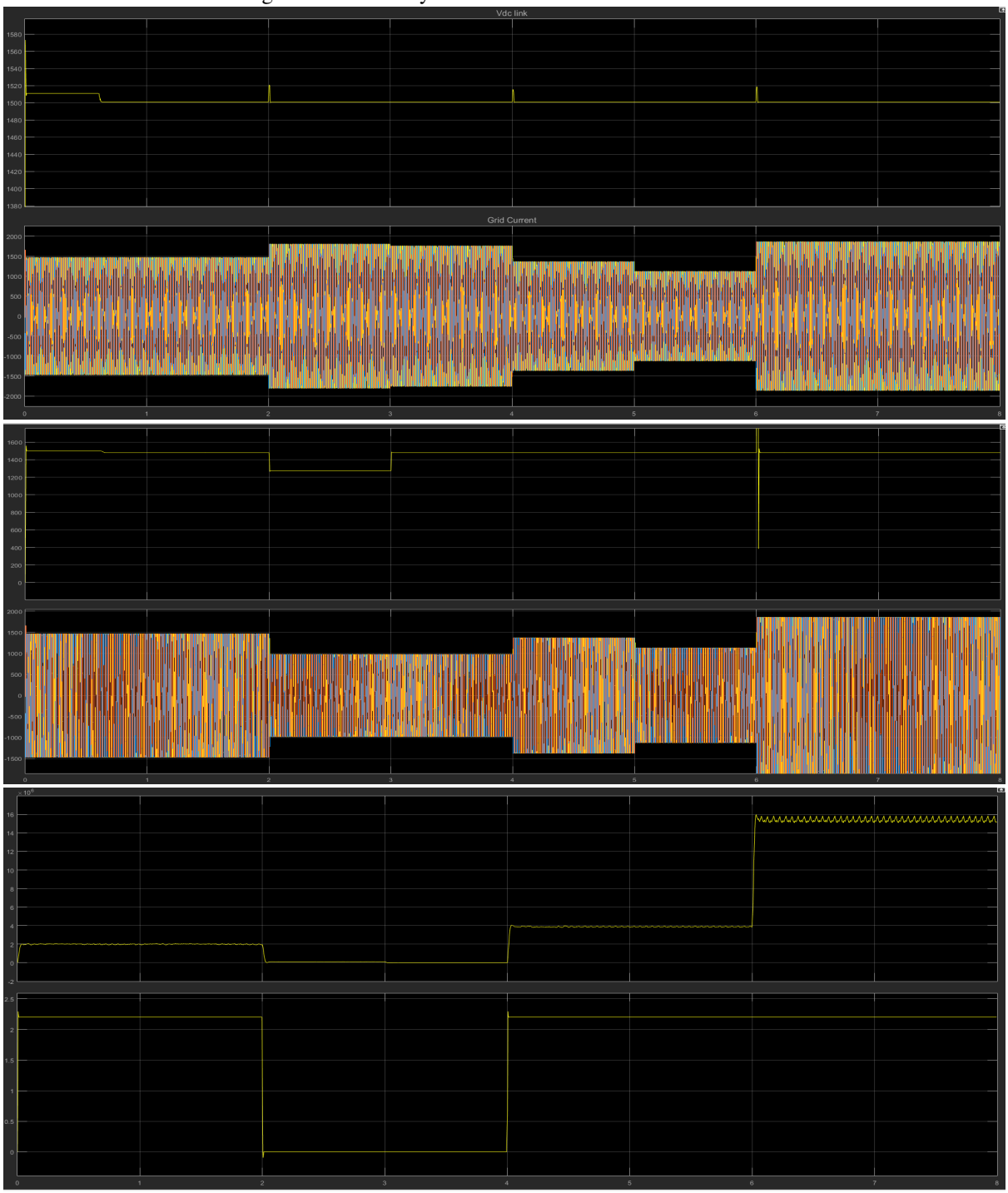

Fig. 7. Performance of the wind generator only. (a) DC-link voltage. (b) Wind and solar generated powers. (c) Injected ac current to the utility-grid.

D. PV-Only Generation

The wind speed is assumed to be less than the cut-off speed, and hence the majority of the generated wind power is con sumed in the system losses. Therefore, the PMSG operates in the braking mode and the rotor is brought to a stand-still by mechanical means. As shown in Fig. 7(a), the speed controller is utilized to drop ωr from 1 p.u. to 0, and then back to 1p.u. at t = 2 and 3 s, respectively. This corresponds to a sudden change in the wind power between 0 and 1 p.u. as shown in Fig. 7(b). In spite of the challenging operating scenario, the system stability is maintained.

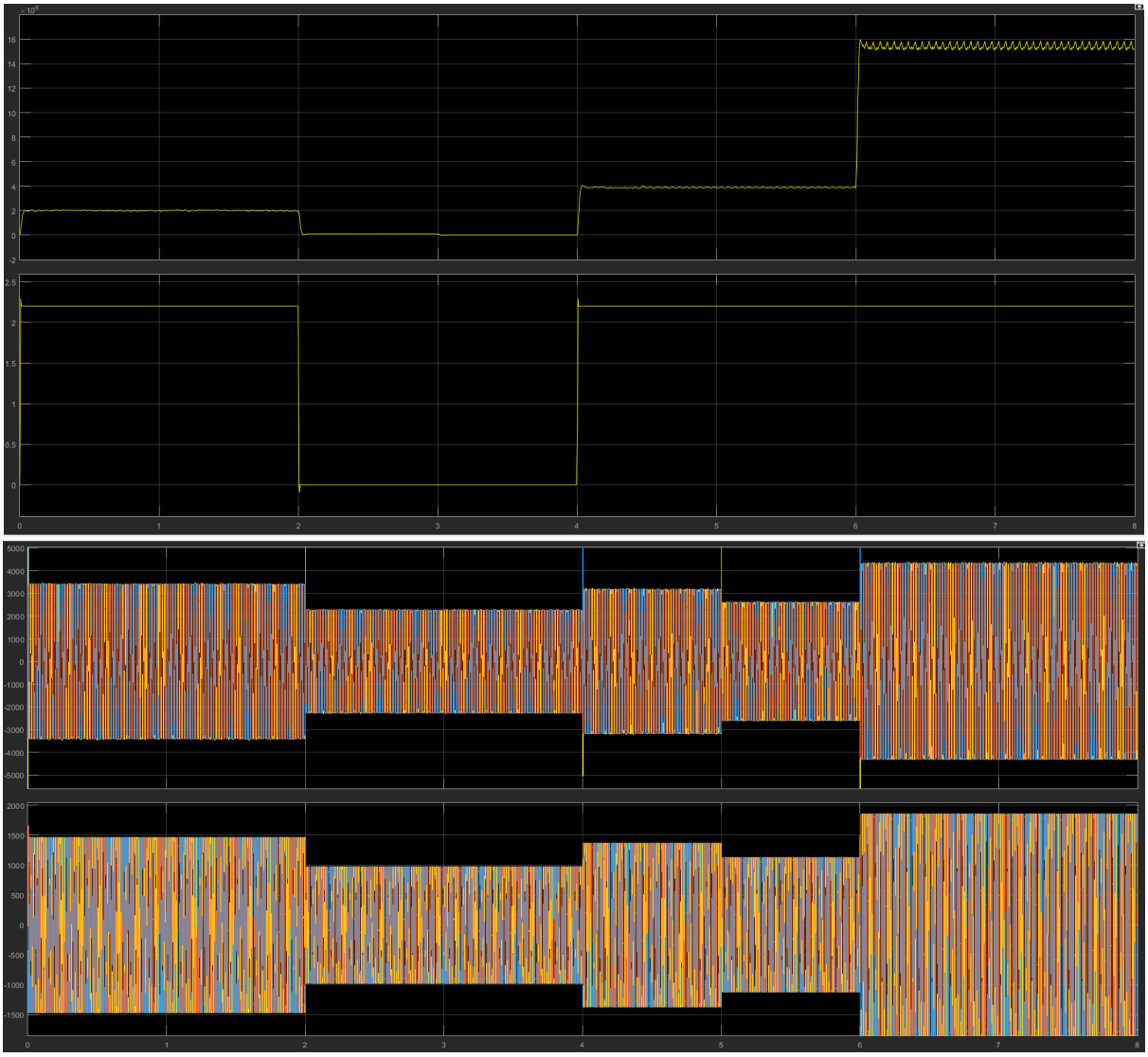

Fig. 8. Performance of the PV generator only. (a) DC-link voltage. (b) Wind and solar generated powers. (c) Injected ac current to the utility-grid.

E. Co-Generation under Utility-Grid Faults Conditions

Converter-based distributed generation units roughly contribute by the rated currents under the short circuit conditions. Therefore, and due to the increased penetration of the renewable energy resources to the electrical grids, some utilities have enforced the fault-ride through of power converters [32]. Accordingly, the distributed plants must not disconnect during a voltage drop down to 0 p.u. that continues to less than or equal to 150 ms (9 cycles for 60 Hz systems). In this operational scenario, the proposed hybrid wind-solar system is investigated for the fault-ride-through capabilities. The PCC in Fig. 1 has been subjected to a 3PG fault at t = 4 s for 4.0 cycles. Further, the VSCs have been implemented in the Simulink model using pulse-width-modulated switching blocks. Fig. 8 shows the performance of the dc-link and the utility-grid current under the 1.0 p.u. and 0.5 p.u wind power generation whereas the solar power generation is maintained at 1.0 p.u. At 1.0 p.u. wind and solar power generation, and after the clearance of the 3PG fault,

the dc-link voltage stability is violated whereas the quality of the injected ac current is degraded with a THD of 8.75%. On the contrary, the response with the 0.5 and 1.0 p.u. wind and solar power generation, respectively, reflects a stable dc-link voltage and a better current quality with a THD of 3.61%. This implies that the wind generator is associated with the system instabilities under the utility-grid faults conditions. The fault conditions induce a sudden drop in the PCC voltage that hinders the maximum power transfer from the dc-link to the grid. As the input wind power is driven by a relatively slow mechanical system, the wind power is therefore kept injected to the dc-link capacitor such that the dc-link voltage increases at the fault instant as shown in Fig. 8(a). On the contrary, the PV generator does not contribute to the dc-link voltage instabilities under the fault conditions. The increased dc-link voltage relocates the operating points of the PV array beyond the maximum power point, as shown in Fig. 3, where the corresponding generated PV power is significantly reduced.

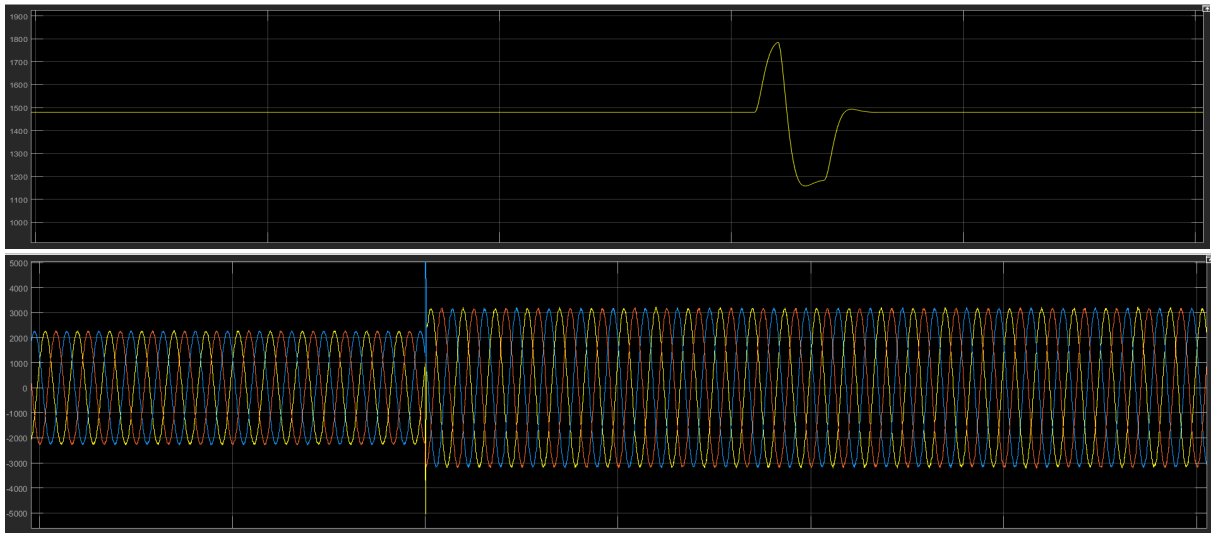

Fig. 9. Response to a 3PG fault at t = 4.0 s for 4.0 cycles – 1.0 and 0.5 p.u. wind power generation with 1.0 p.u. solar power.

Therefore, the PV generator has self-healing capabilities under the utility-grid faults conditions. In the literature, the protection against the fault conditions in the PMSG wind generators has been achieved by activating the following protection schemes at the utility-grid fault conditions [33]; 1) using a braking resistance in parallel to the dc-link capacitor so that the generated wind power can be dissipated during the faults. 2) using the pitch angle control so that the wind turbine blades are twisted to reduce the amount of wind power extraction, and hence the input mechanical torque to the PMSG is reduced. Note that both approaches can be used so that the braking resistance provides a quick damping till the mechanical pitch controller is activated. Fig. 9 shows the system performance when the preceding fault protections are implemented under 1.0 p.u. wind and solar power generation. The increase of the dc-link voltage has been limited whereas the injected ac current to the grid is maintained stable. The fault-ride through has been enabled by dissipating the wind power into the braking resistance and reducing the generated wind power using the pitch angle control, and so the input-output power balance across the dc-link capacitor is achieved. For further investigations, the system performance under the single-phase-to-ground (1PG) fault conditions is investigated in Fig. 10. It is clear that the 1PG fault is not detrimental to the system performance as compared to the 3PG faults in Fig. 8. However, the protected system in Fig. 10 reflects a more damped dc-link response as compared to the unprotected scenario.

Fig. 10. Response to a 3PG fault at t = 4.0 s for 4.0 cycles – 1.0 p.u. wind and solar power generation with implemented fault protection schemes.

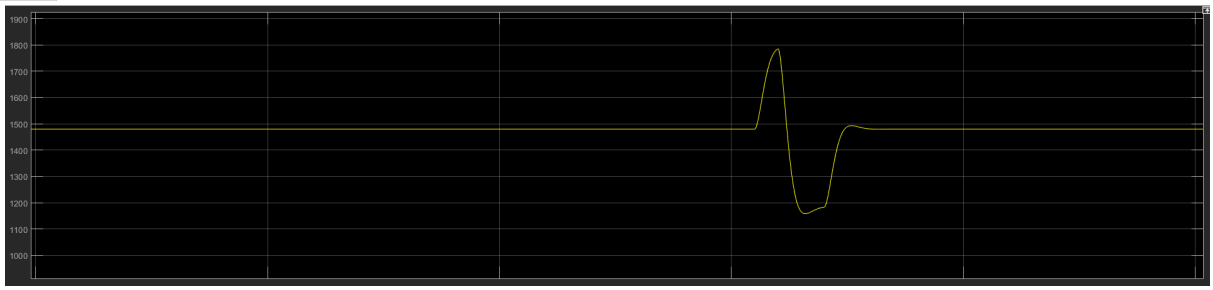

Fig. 11. Response to a 1PG fault at t = 4.0 s for 4.0 cycles – 1.0 p.u. wind and solar power generation with and without the fault protection schemes.

F. Co-Generation under Parameters Variation – Robustness

It is shown in Fig. 5 that the system performance is stable under wide variation range of operating points. In this section, the system performance is evaluated against the parameters variations. The short-circuit-ratio (SCR) is a quantity characterizing the stiffness of the utility-grid, where SCR is the ratio of the shortcircuit capacity of the utility-grid at the PCC to the rated dc power of the interconnected power converter. In this paper, the utility-grid is originally assumed strong with SCR = 15 [results in Fig. 5]. In this section, the SCR has decreased to 4.0 and 2.3 to challenge the interconnected converter, as shown in Fig. 11. In both cases, the solar power is maintained at 1.0 p.u. whereas the wind power is subjected to a step increase from 0.5 to 1.0 p.u. at t = 1 s. The system response is stable at a wide variation range of SCR values from SCR = 15 to SCR = 4.5 as shown in Figs. 5 and 11, respectively. However, the system becomes unstable at SCR = 2.3 which is expected at the very weak grid conditions due to the interaction with the PLL dynamics [7]. Under the same operating conditions, the influence of the variations of Cf on the grid voltage is investigated in Fig. 12. As shown, the total harmonic distortion (THD) for the PCC voltage increases from 0.05% to 9.8% at 1.25 and 1.5Cf , respectively. In spite of using simple PI controllers for the proposed system, the results in Fig. 11and 12 indicate a reasonable robustness against the utility-grid parameters variations

IV. CONCLUSION

This paper has presented the combination of the wind and solar systems using vector-controlled grid-connected BtB VSCs. The VSR at the wind generator side is responsible for extracting the maximum wind power following the wind velocity variations. On the utility-grid side, the roles of the VSI are to extract the maximum PV power from the PV generator, achieve the balance between the input and output powers across the dc-link capacitor, and to maintain a unity PCC voltage under different modes of operation. A small-signal linearization analysis has been conducted where the entire state-space model is developed to investigate the system stability. The proposed system features the following advantages; 1) the increased reliability and efficiency due to the combined wind and solar generators. 2) the independent MPPT extraction as the VSR and VSI are solely responsible for extracting the wind and PV powers, respectively. 3) the regulation of the dc-link voltage under all operating conditions is maintained by the VSI and hence a better damped performance is yielded. 4) simple system structure and controllers design. 5) fault-ride through can be achieved using existing protection schemes. A well-damped performance and an efficient operation have been revealed from the time-domain simulations results under the Matlab/Simulink environment under different operational scenarios.

REFERENCES

[1] Renewable Energy Policy Network for the 21st Century, “Advancing the global renewable energy transition,” REN21 Secretariat, Paris, France, 2017. [Online]. Available: http://www.ren21.net/wpcontent/uploads/2017/06/GSR2017_-Highlights.pdf

[2] F. Blaabjerg, Z. Chen, and S. B. Kjaer, “Power electronics as efficient interface in dispersed power generation systems,” IEEE Trans. Power Electron., vol. 19, no. 5, pp. 1184–1194, Sep. 2004.

[3] J. Carrasco et al., “Power-electronic systems for the grid integration of renewable energy sources—a survey,” IEEE Trans. Ind. Electron., vol. 53, no. 4, pp. 1002–1016, Jan. 2006.

[4] A. Yazdani and P. P. Dash, “A control methodology and characterization of dynamics for a photovoltaic (PV) system interfaced with a distribution network,” IEEE Trans. Power Del., vol. 24, no. 3, pp. 1538–1551, Jul. 2009.

[5] L. Nousiainen et al., “Photovoltaic generator as an input source for power electronic converters,” IEEE Trans. Power Electron., vol. 28, no. 6, pp. 3028–3038, Jun. 2013.

[6] N. Strachan and D. Jovcic, “Stability of a variable-speed permanent magnet wind generator with weak ac grids,” IEEE Trans. Power Del., vol. 25, no. 4, pp. 2279–2788, Oct. 2010.

[7] P. Mitra, L. Zhang, and L. Harnefors, "Offshore wind integration to a weak grid by VSC-HVDC links using power-synchronization control— A case study," IEEE Trans. Power Del., vol. 29, no. 1, pp. 453–461, Feb. 2014.
[8] Y. Wang, J. Meng, X. Zhang, and L. Xu, "Control of PMSGbased wind turbines for system inertial response and power oscillation damping," IEEE Trans. Sustain. Energy, vol. 6, no. 2, pp. 565–574, Apr. 2015.
[9] F. Giraud, "Analysis of a utility-interactive wind-photovoltaic hybrid system with battery storage using neural network," Ph.D. dissertation, Dept. Electr. Eng., Univ. Massachusetts Lowell, Lowell, MA, USA , 1999.
[10] L. Xu, X. Ruan, C. Mao, B. Zhang, and Y. Luo, "An improved optimal sizing method for wind-solar-battery hybrid power system," IEEE Trans. Sustain. Energy, vol. 4, no. 3, pp. 774–785, Jul. 2013.
[11] S. Sarkar and V. Ajjarapu, "MW resource assessment model for a hybrid energy conversion system with wind and solar resources," IEEE Trans. Sustain. Energy, vol. 2, no. 4, pp. 383–391, Oct. 2011.
[12] Y.-M. Chen, Y.-C. Liu, S.-C. Hung, and C.-S. Cheng, "Multi-input inverter for grid-connected hybrid PV/wind power system," IEEE Trans. Power Electron., vol. 22, no. 3, pp. 1070–1077, May 2007.
[13] S. Bae and A. Kwasinski, "Dynamic modeling and operation strategy for microgrid with wind and photovoltaic resources," IEEE Trans. Smart Grid, vol. 3, no. 4, pp. 1867–1876, Dec. 2012.
[14] B. Mangu, S. Akshatha, D. Suryanarayana, and B. G. Fernandes, "Grid-connected PV-wind-battery-based multi-input transformer-coupled bidirectional dc-dc converter for household applications," IEEE Trans. Emerg. Sel. Topics Power Electron., vol. 4, no. 3, pp. 1086–1095, Sep. 2016.
[15] P. Shanthi, G. Uma, and M. S. Keerthana, "Effective power transfer scheme for a grid connected hybrid wind/photovoltaic system," IET Renew. Power Gener., vol. 11, no. 7, pp. 1005–1017, 2017.

AUTHORS DETAILS

Mrs. J. Sravanthi receive d the B. Tech Degree in Electrical and Electronics Engineering Teegala Krishna Reddy Engineering College Meerpet, Near LB Nagar Hyderabad (Dist), Telangana, India. And Studying M. tech in the Dept. of Electrical & Electronics Engineering, in Power Electronics at Holy Mary Institute of Technology and Science, Bogaram(V), Medchal (D), Hyderabad, India.

Mrs. A. Anuradha received the B. TECH degree in EEE from Christu jyothi institute of Technology, Yeshwanthapur, jangaon, Telangana, INDIA, from JNTU University and MTECH in Electrical Power Systems in Vignan Bharati institute of technology and sciences, near Ghatkesar Bogaram (v), Medchal Dist, Hyderabad, Telangana, INDIA. She has 2 years of teaching experience, currently working as Assistant professor at Holy Mary Institute of Technology and sciences, Bogaram, Medchal District, Hyderabad, Telangana, INDIA in EEE department. Her interest areas are Electrical power systems.

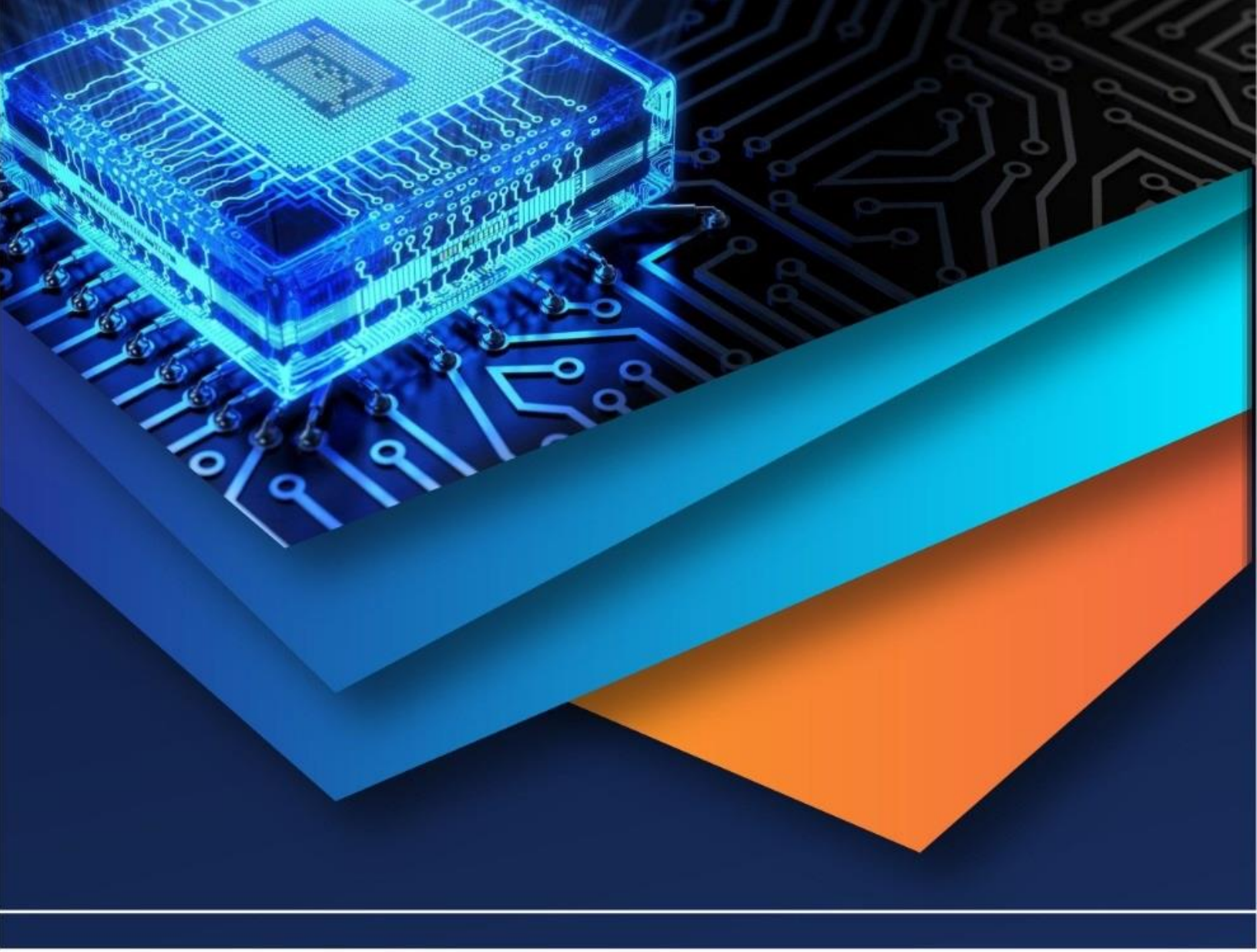

10.22214/IJRASET

45.98

IMPACT FACTOR: 7.129

IMPACT FACTOR: 7.429

INTERNATIONAL JOURNAL FOR RESEARCH

IN APPLIED SCIENCE & ENGINEERING TECHNOLOGY